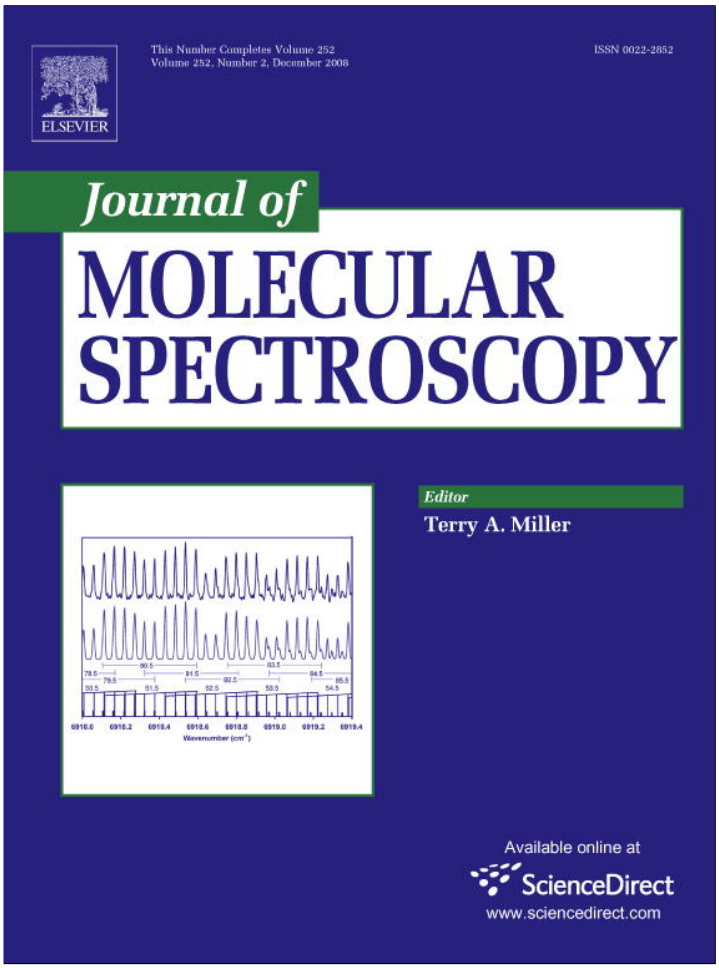

Journal of Molecular Spectroscopy 252 (2008) 108–114

Contents lists available at ScienceDirect

Journal of Molecular Spectroscopy

journal homepage: www.elsevier.com/locate/jms

Determination of vibrational energy levels and transition dipole moments of CO_2 molecules by density functional theory

Zhi Liang, Hai-Lung Tsai *

Department of Mechanical and Aerospace Engineering, Missouri University of Science and Technology (formerly University of Missouri-Rolla), Rolla, MO 65409, USA

ARTICLE INFO

Article history:
Received 22 May 2008
In revised form 26 June 2008
Available online 25 July 2008

Keywords:
CO_2
DFT
PW basis functions
Transition dipole moment

ABSTRACT

An efficient method is presented to calculate the intra-molecular potential energies and electrical dipole moments of CO_2 molecules at the electronic ground state by solving the Kohn–Sham (KS) equation for a total of 101 992 nuclear configurations. The projector-augmented wave (PAW) exchange-correlation potential functionals and plane wave (PW) basis functions were used in solving the KS equation. The calculated intra-molecular potential function was then included in the pure vibrational Schrödinger equation to determine the vibrational energy eigen values and eigen functions. The vibrational wave functions combined with the calculated dipole moment function were used to determine the transition dipole moments. The calculated results were compared with the experimental data.

1. Introduction

Two important problems in the study of infrared absorption spectrum are to determine vibrational energy levels and molecular transition dipole moments. To obtain these results, it is necessary to calculate the intra-molecular potential energy surface (PES) and molecular dipole moment surface (DMS) by ab initio methods. The ab initio calculations of PESs and DMSs of tri-atomic molecules were implemented in several papers [1–7] by the coupled-cluster singles and doubles excitation with perturbative treatment of triple excitations [CCSD(T)] [8] method and the multi-reference configuration interaction (MRCI) method. Localized basis sets such as augmented correlation-consistent polarized quadruple zeta (aug-cc-pVQZ) functions were used in these calculations. Using these methods and basis sets, the potential energies and dipole moments were usually evaluated at 10^2–10^3 different nuclear configurations that are close to the molecular equilibrium structures. The data were then fitted by polynomial expansions in displacement coordinates, and used in the calculations of molecular properties. In some calculations [2], the coefficients in polynomial expansions needed to be optimized in order to accurately reproduce the experimental values of fundamental transition energies. Generally, the CCSD(T) and MRCI methods combined with localized basis sets gives accurate calculated results. But the method is very computationally demanding.

In this paper, density functional theory (DFT) was used to determine the electronic ground state potential energy of the CO_2 molecule. Using DFT, the many-electron Schrödinger equation could be transformed to an effective one electron Schrödinger equation, i.e., Kohn–Sham (KS) equation. There are two critical problems in solving the KS equation; one is to find appropriate exchange-correlation functionals, and the other is to choose appropriate basis functions. In the calculations, projector-augmented wave (PAW) potentials [9,10] and plane wave (PW) basis sets were used. DFT method with PW basis sets has several advantages over CCSD(T) method with localized basis functions. These include:

(i) In DFT, the ground-state electronic energy and dipole moment are uniquely determined by the ground-state charge density which is a function of only three variables. Compared to methods such as CCSD(T), DFT reduces the computational cost so that more configurations of small molecules can be evaluated and rather larger molecules are able to be handled.
(ii) The KS equations take on a very simple form if PW basis functions are used. The well-developed numerical schemes for the Fourier transforms can be used to evaluate the Hamiltonian matrix elements so that much computational time is saved.
(iii) Compared to localized basis sets, no basis-set corrections to forces are needed for PW basis sets because PW basis sets do not depend on nuclear positions. Hence, the PW basis sets allow for relatively simple calculations of forces in the determinations of molecular equilibrium geometries.
(iv) The same PW basis sets can be used for all atomic species [11].

Due to the high efficiency of the calculation method we use, intra-molecular potential energies and molecular dipole moments

* Corresponding author.
E-mail address: tsai@mst.edu (H.-L. Tsai).

0022-2852/$ - see front matter © 2008 Elsevier Inc. All rights reserved.
doi:10.1016/j.jms.2008.07.008

were evaluated at more than 10^5 different nuclear configurations so that the PES and MDS could be constructed without interpolations or fitting to polynomial expansions. However, there are some problems we need to consider in the calculations if we want to implement PW basis functions to an aperiodic system like an isolated molecule [12]. The problems will be discussed Section 2. Appropriate parameters should be selected to make a compromise between computational time and accuracy.

By solving the KS equation, both the intra-molecular PES and molecular MDS were obtained. The calculated potential energy function was included in the vibrational Schrödinger equation. To efficiently solving the vibrational Schrödinger equation, we split the four-variable potential energy function into four one-variable potential functions that correspond to the potential functions of four vibrational normal modes of CO_2 and one perturbation function. The four one-dimensional Schrödinger equations were then obtained by the separation of variables. The solutions of these Schrödinger equations were used as the 0th order results. The perturbation function was then included to obtain the real vibrational energy eigen values and wave functions. These results combined with calculated dipole moment functions were used to calculate the molecular transition dipole moments. The calculated results were compared with the experimental values. The details are shown in Section 3.

2. Potential and dipole moment surfaces

In the first step, we calculate the intra-molecular potential energy and molecular dipole moment as a function of CO_2 nuclear configurations. Using the density functional theory, the Born–Oppenheimer potential energy at each nuclear configuration can be determined by solving an effective one electron Schrödinger equation (i.e., KS equation [13]) as

$$\hat{H}^{KS}\psi_i^{KS}(1) = \varepsilon_i^{KS}\psi_i^{KS}(1) \tag{1a}$$

where

$$\hat{H}^{KS} = -\frac{1}{2}\nabla_1^2 \underbrace{-\sum_A \frac{Z_A}{\vec{r}_{iA}} + \int \frac{\rho(\vec{r}_2)}{r_{12}}\,\mathrm{d}\vec{r}_2 + v_{xc}(1)}_{V_{eff}(\vec{r})} \tag{1b}$$

In Eq. (1), $\psi^{KS}(1)$ is the one electron wave function and $\rho(\vec{r}) = \sum_{i=1}^{n}|\psi_i^{KS}|^2$ is the electron charge density function. If this equation is solved, the charge density distribution $\rho(\vec{r})$ is also known. $\rho(\vec{r})$ can then be used in the calculation of the molecular dipole moment by the following equation:

$$\vec{d}(\{\vec{R}\}) = \int \mathrm{d}\vec{r}\,\rho(\vec{r})\cdot\left(\vec{r} - \vec{R}_{center}\right) \tag{2}$$

where: $\{\vec{R}\}$ denotes the nuclear configuration of the molecule $\vec{R}_{center}$ is the center of the molecule. Note Eq. (1) is written in atomic units. $\vec{R}_{center}$ is the center of the molecule. Note Eq. (1) is written in atomic units.

The first three terms in the Hamiltonian of the KS equation, i.e., the electronic kinetic energy, the electron–nuclear attraction potential, and the electron–electron repulsive potential all have explicit forms. However, the last potential term v_{xc}, i.e., the exchange-correlation potential is unknown. Some approximations must be made to obtain an appropriate v_{xc}. In our calculations, we used a PAW potential (pseudopotentials were used to represent the core electrons), which is supplied by the Vienna Ab Initio Simulation Package (VASP) [14,15].

Now the problem turns to how to select the basis functions. The basis functions should be chosen so that the wave function ψ_i^{KS} satisfies proper boundary conditions. In our calculations the CO_2 molecule was placed in the center of a cubic supercell of side L as shown in Fig. 1. In order to use PW functions as basis functions, periodic boundary conditions (PBC's) were applied. So the one electron wave function can be written as

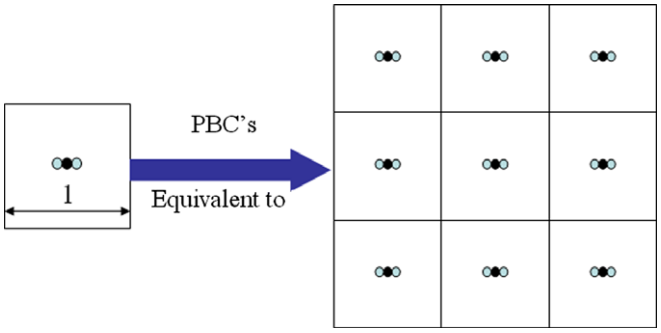

Fig. 1. A CO_2 molecule in a cubic supercell with PBC's.

$$\psi(\vec{r}) = \sum_{\vec{K}} \alpha\left(\vec{K}\right)\mathrm{e}^{\mathrm{i}\vec{K}\cdot\vec{r}} \tag{3}$$

where $\vec{K}\cdot\vec{l} = 2\pi m$, m is an integer, $\vec{K}$ is a wave vector, and $\vec{l}$ is a lattice vector. The PW functions have a big advantage in solving KS equations because the Hamiltonian matrix elements now become [16] $\hat{H}_{\vec{K}'\vec{K}} = \frac{1}{V_c}\int \mathrm{d}\vec{r}_1(\mathrm{e}^{\mathrm{i}\vec{K}'\cdot\vec{r}})^*\hat{H}^{KS}(1)\,\mathrm{e}^{\mathrm{i}\vec{K}\cdot\vec{r}}$, where V_c is the volume of the cubic supercell which is used as the normalization factor. In Eq. (1), we know

$$\hat{H}^{KS} = -\frac{1}{2}\nabla_1^2 + V_{eff}(\vec{r}) \tag{4a}$$

Hence

$$\hat{H}_{\vec{K}'\vec{K}} = \frac{\vec{K}^2}{2}\delta_{\vec{K}\vec{K}'} + \frac{1}{V_c}\int V_{eff}\,\mathrm{e}^{\mathrm{i}(\vec{K}-\vec{K}')\cdot\vec{r}}\,\mathrm{d}\vec{r} \tag{4b}$$

One can see that the second part of Eq. (4b) is the Fourier transform of an effective potential which can be easily evaluated by the well-developed numerical schemes.

In the implementation, the PW basis functions must be truncated at some wave number $\vec{K}$. This wave number should be high enough to account for some fast oscillating components of the electronic wave functions. In the calculation, cut-off energy was used to control the number of basis functions, and the relation is shown in the following equation:

$$\frac{\hbar^2K^2}{2m_e} = \frac{\hbar^2\left(\frac{2\pi}{L}\right)^2(N_x^2+N_y^2+N_z^2)}{2m_e} < E_{cut} \tag{5}$$

where N_i is the number of basis functions in i-direction. From Eq. (5) one can see the number of basis functions is determined by both the supercell size L and cut-off energy E_{cut}. A large L or E_{cut} corresponds to a large number of basis functions. A large number of basis functions correspond to a high accuracy and computational cost. Hence, one must pick the appropriate supercell size and cut-off energy to make a compromise between accuracy and computation cost.

2.1. Choose appropriate supercell size

Although the PBC's with PW basis functions could save much computational time, this method brings one problem in the calculations of isolated molecules. As shown in Fig. 1, there exist spurious interactions of aperiodic charge density with its images in the neighboring supercells. The potential energy $E(L)$ calculated in a finite cubic supercell with side L differs from the potential energy calculated in the limit $E_0 = E(L\to\infty)$. To estimate E_0 from the calculated $E(L)$, one needs to know the asymptotic dependence of E on L.

It was proved [12] that the asymptotic behavior of an isolated neutral molecule without dipole moment in a cubic supercell can be determined by the quadrupole–quadrupole interaction, which has a functional dependence of L^{-5}. We calculated the equilibrium C–O separation r_e and the minimal potential energy U_{min} of the molecule at different supercell sizes. The calculations were performed using the program VASP. The cut-off energy was chosen as 1000 eV. The results were shown in Fig. 2, where one can see that both U_{min} and r_e converge very fast with the supercell size. The calculated r_e is 1.162 Å which is very close to the experimental value [17] 1.160 Å.

However, a CO_2 molecule only has zero dipole moment at symmetric linear configurations. When the molecule deviates from its equilibrium configuration, it could have dipole moment. In this case, the asymptotic dependence of potential energy on supercell size is dominated by a dipole-dependent term $\frac{2\pi}{3V_c}\left|\int_{cell} d^3r\, \vec{r}\, \rho(\vec{r})\right|^2$. The absence of this dipolar term could lead to a $O(L^{-3})$ convergence [12]. Fig. 3 shows the potential energy of asymmetric stretching a CO_2 molecule by 0.15 Å from equilibrium as a function of supercell size. The calculations were performed both with and without the dipolar term, and the results are shown in Fig. 3. One can see the two curves converge to the same value; but the calculation with the dipolar term converges faster than the one without the dipolar term. So, to get a result with the same accuracy, we need to use a relatively larger supercell size if we do not include the dipolar term. However, larger supercell size means more computational time. To save the computational time, we always include the dipolar term in our calculations.

From the above analysis, to make a compromise between computation time and accuracy, we chose a cubic supercell size of 10 Å in our calculations. The dipolar potential term is always included.

2.2. Choose appropriate cut-off energy

We fix the supercell size at 10 Å and change the cut-off energy from 700 to 1300 eV. The minimal potential energy of a CO_2 molecule and the dipole moment at the nuclear configuration of asymmetric stretching the molecule by 0.2 Å from equilibrium were calculated. The results were shown in Fig. 4. The molecule has bigger dipole moments and lower potential energies at larger cut-off energies. Note the values only change a little (less than 0.1%) after 1000 eV and hence 1000 eV was chosen as the cut-off energy in our calculations.

One can see the PW basis functions only depends on supercell sizes. They do not depend on atomic species in the molecule or nuclear positions. The convergence properties with respect to supercell size and cutoff energy can be easily tested by the above calculations. The computational cost of the test procedure is very small compared to later calculations of PES and MDS. Once the appropriate supercell size and cutoff energy are chosen, one could keep these parameters constant and calculate potential energies and dipole moments at different configurations with a good accuracy and efficiency.

By placing the CO_2 molecule at the center of a cubic supercell of side 10 Å, choosing the cut-off energy at 1000 eV, and including the dipolar potential term, we calculated the intra-molecular potential and molecular dipole moment at 101 992 different nuclear configurations. The details of these configurations are shown in Table 1. The calculated potential energy and dipole moment surfaces will be used in the next section to determine the vibrational energy levels and transition dipole moments.

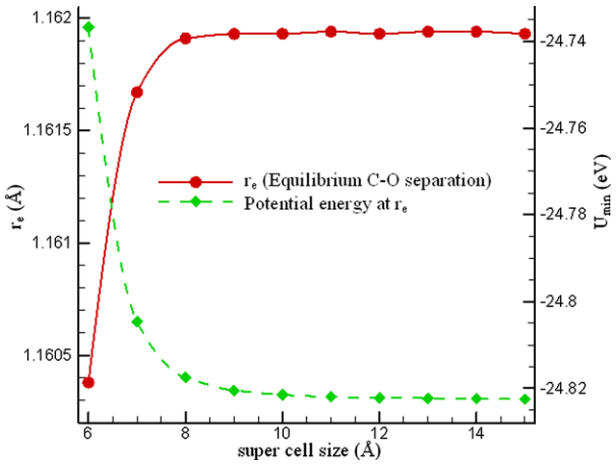

Fig. 2. r_e and U_{min} vs. supercell size.

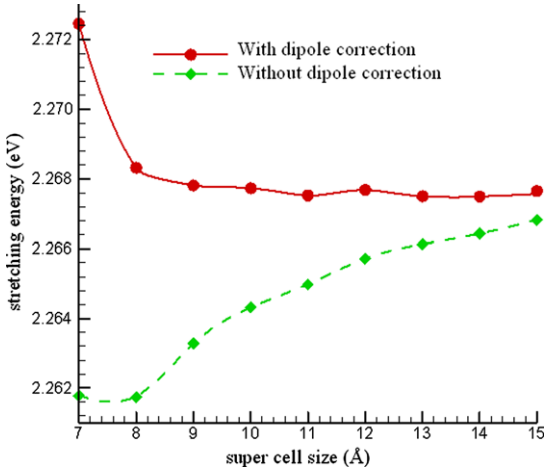

Fig. 3. Potential energy of stretching a CO_2 with and without dipole-dependent term.

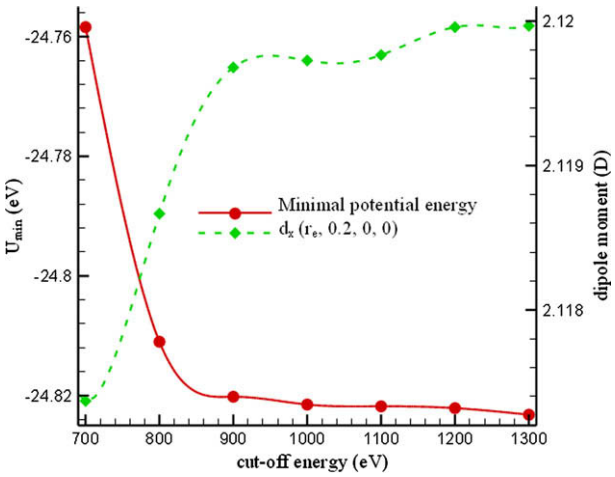

Fig. 4. U_{min} and dipole moment vs. E_{cut}.

Table 1
Values of *r*, *x*, *y*, and *z* used in the calculations

	Variation (Å)	Increment (Å)	Number of points
r	2.10–2.58	0.008	61
x	0–0.172	0.004	44
y or *z*	0–0.37	0.01	38

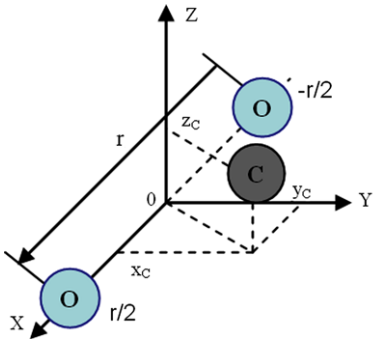

Fig. 5. Coordinates of a CO_2 molecule.

3. Vibrational levels and transition dipole moment

Using the coordinate system as shown in Fig. 5, the pure vibrational Schrödinger equation of a CO_2 molecule can be expressed as

$$\hat{H}_v\psi = E\psi \tag{6a}$$

where

$$\hat{H}_v = -\frac{\hbar^2}{2\mu_O}\frac{\partial^2}{\partial r^2} - \frac{\hbar^2}{2\mu_C}\left(\frac{\partial^2}{\partial x^2}+\frac{\partial^2}{\partial y^2}+\frac{\partial^2}{\partial z^2}\right) + U(r,x,y,z) \tag{6b}$$

In Eq. (6), r represents the distance between two O atoms; x, y and z are the three components of the vector starting from the middle point of the two O atoms and ending at the C atom; U is the potential term; μ_O and μ_C are, respectively, the reduced mass of O atom and C atom and they are given by the following equation:

$$\mu_O = \frac{m_O}{2}, \quad \mu_C = \frac{m_C \cdot 2m_O}{m_C + 2m_O} \tag{7}$$

The potential energy term depends on four variables. However, y and z are actually equivalent due to the symmetry of the CO_2 molecule. So in the construction of potential and dipole moment surface, to save computational time, we fixed the z to be 0 and changed the values of the other three variables. After we get the functions $U(r,x,y,0)$ and $d(r,x,y,0)$, the full surface of the potential and dipole moment, i.e., $U(r,x,y,z)$ and $d(r,x,y,z)$ can be obtained according to the symmetry.

Fig. 6(a)–(c) shows the iso-surfaces of $U(r,x,y,0)$, x component of $d(r,x,y,0)$ and y component of $d(r,x,y,0)$, respectively. The z component of $d(r,x,y,0)$ is not shown because it is always 0. Note in Fig. 6, the unit of U is eV, and the unit of dipole moment is

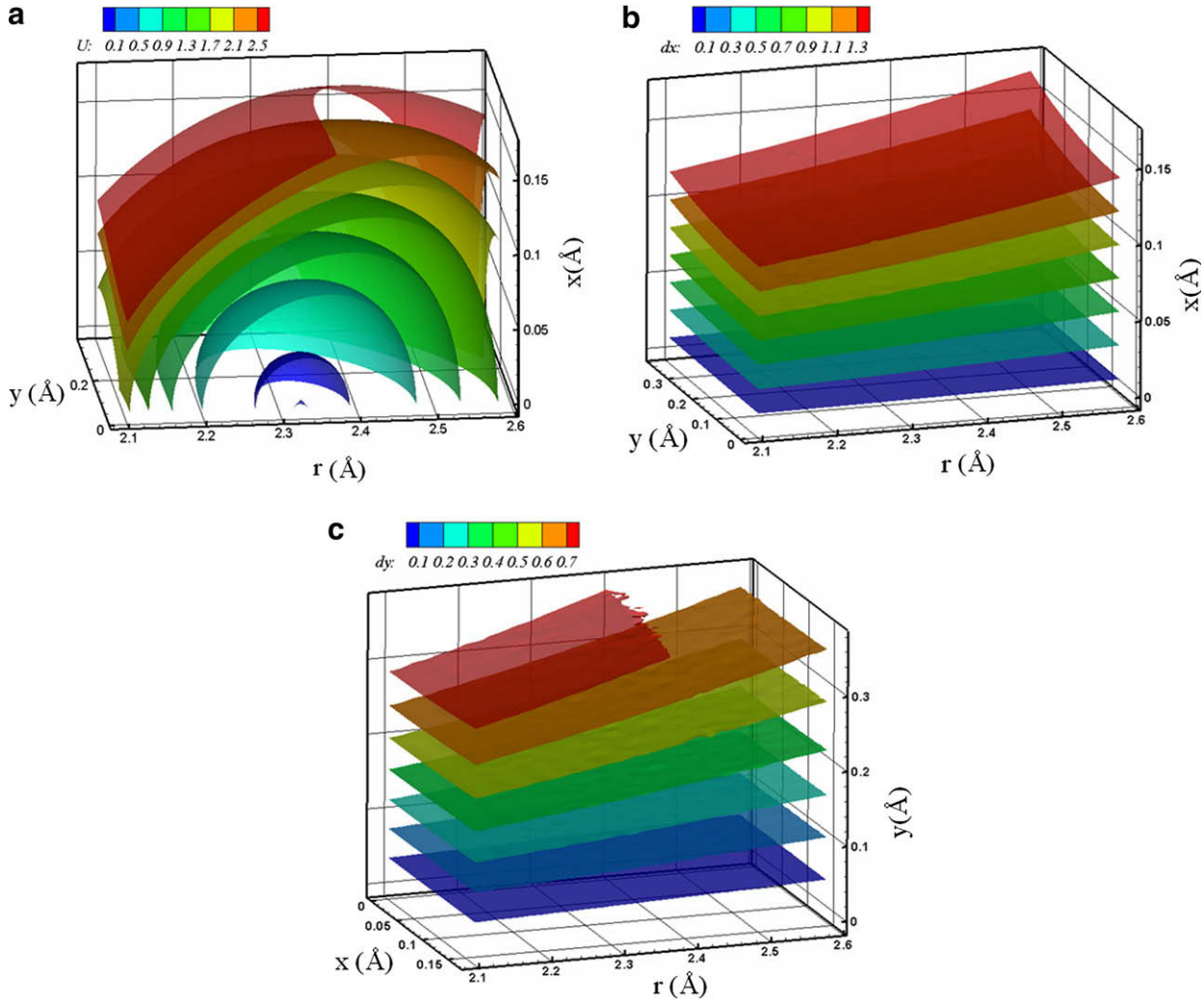

Fig. 6. Iso-value surfaces of (a) intra-molecular potential energy $U(r,x,y,0)$; (b) dipole moment component parallel to the molecular axis $d_x(r,x,y,0)$; and (c) dipole moment component perpendicular to the molecular axis $d_y(r,x,y,0)$.

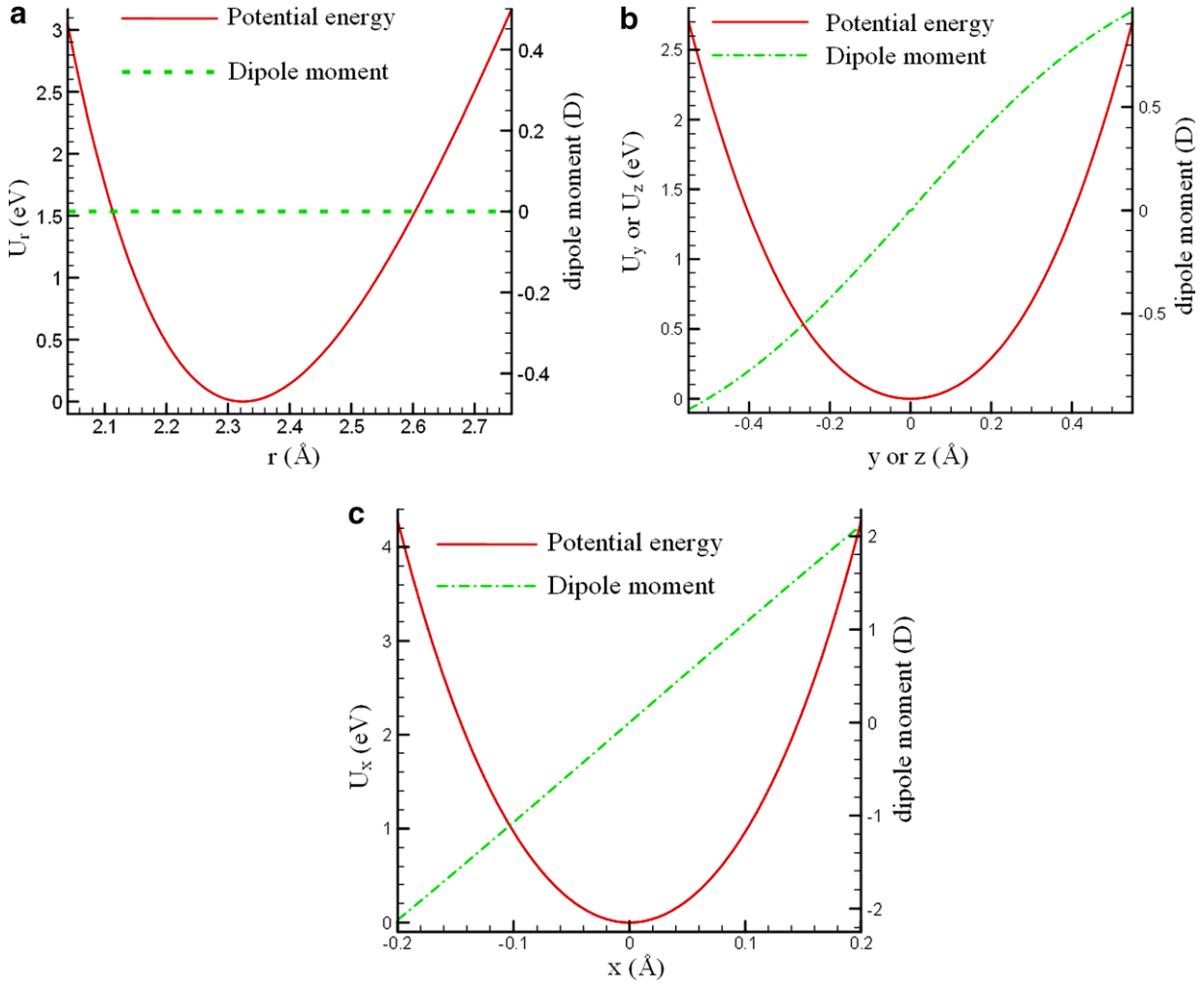

Fig. 7. Intra-molecular potential energy and dipole moment functions of (a) $U(r,0,0,0)$ and $d_x(r,0,0,0)$, (b) $U(r_e,0,y,0)$ and $d_y(r_e,0,y,0)$, and (c) $U(r_e,x,0,0)$ and $d_x(r_e,x,0,0)$.

Debye. The zero potential in Fig. 6(a) corresponds to the minimal potential of a CO_2 molecule which is equal to −24.2815 eV.

As Eq. (6) is a four-dimensional Schrödinger equation, in order to solve the equation efficiently, we split $U(r,x,y,z)$ into five parts as follows:

$$U(r,x,y,z) = U_r(r,0,0,0) + U_x(r_e,x,0,0) + U_y(r_e,0,y,0) + U_z(r_e,0,0,z) + V(r,x,y,z) \quad (8)$$

where r_e is the equilibrium C–O separation which is a constant. The first four potential functions on the right-hand side of Eq. (8) are a function of only one variable which can be directly extracted from the function $U(r,x,y,z)$. The remaining three variables in each of the four potential functions are fixed at the equilibrium configuration of the molecule. $V(r,x,y,z)$ is the difference between $U(r,x,y,z)$ and the sum of the four one-variable functions. Fig. 7(a)–(c) shows the four calculated potential functions and the dipole moment functions extracted from $U(r,x,y,z)$ and $d(r,x,y,z)$. Fig. 7(a) corresponds to the symmetric stretching vibration mode; Fig. 7(b) corresponds to the two degenerate bending vibration modes; and Fig. 7(c) corresponds to the asymmetric stretching vibration mode. We define a new Hamiltonian as follows:

$$\hat{H}_0 = -\frac{\hbar^2}{2\mu_0}\frac{\partial^2}{\partial r^2} - \frac{\hbar^2}{2\mu_C}\left(\frac{\partial^2}{\partial x^2} + \frac{\partial^2}{\partial y^2} + \frac{\partial^2}{\partial z^2}\right) + U_r(r) + U_x(x) + U_y(y) + U_z(z) \quad (9)$$

Hence, $\hat{H}_v = \hat{H}_0 + V$, where V is a perturbation term.

One can see a Schrödinger equation with the new Hamiltonian can be easily solved by separation of variables. The four separated one-dimensional Schrödinger equations were solved independently by the Numerov [18] method. The lowest three energy eigen values of each mode were shown in Table 2, and their corresponding normalized wave functions were shown in Fig. 8(a)–(c). The combinations of these energy eigen values and eigen functions form the eigen values E_n and eigen functions $|n\rangle$ of $\hat{H}_0$. The relation is shown as

$$|n\rangle = |n_r n_y n_z n_x\rangle = |n_r\rangle \cdot |n_y\rangle \cdot |n_z\rangle \cdot |n_x\rangle$$
$$E_n = E_{n_r} + E_{n_y} + E_{n_z} + E_{nx} \quad (10)$$

In Eq. (10), each eigen function contain four quantum numbers. The first quantum number n_r corresponds to the symmetric stretching

Table 2
Energy eigen values (cm^{-1}) where all the values are subtracted by the corresponding ground state energies

Quantum number	Eigen energy		
	E_{n_r}	E_{n_y} or E_{n_z}	E_{n_x}
0	0	0	0
1	1344	662	2430
2	2682	1332	4879

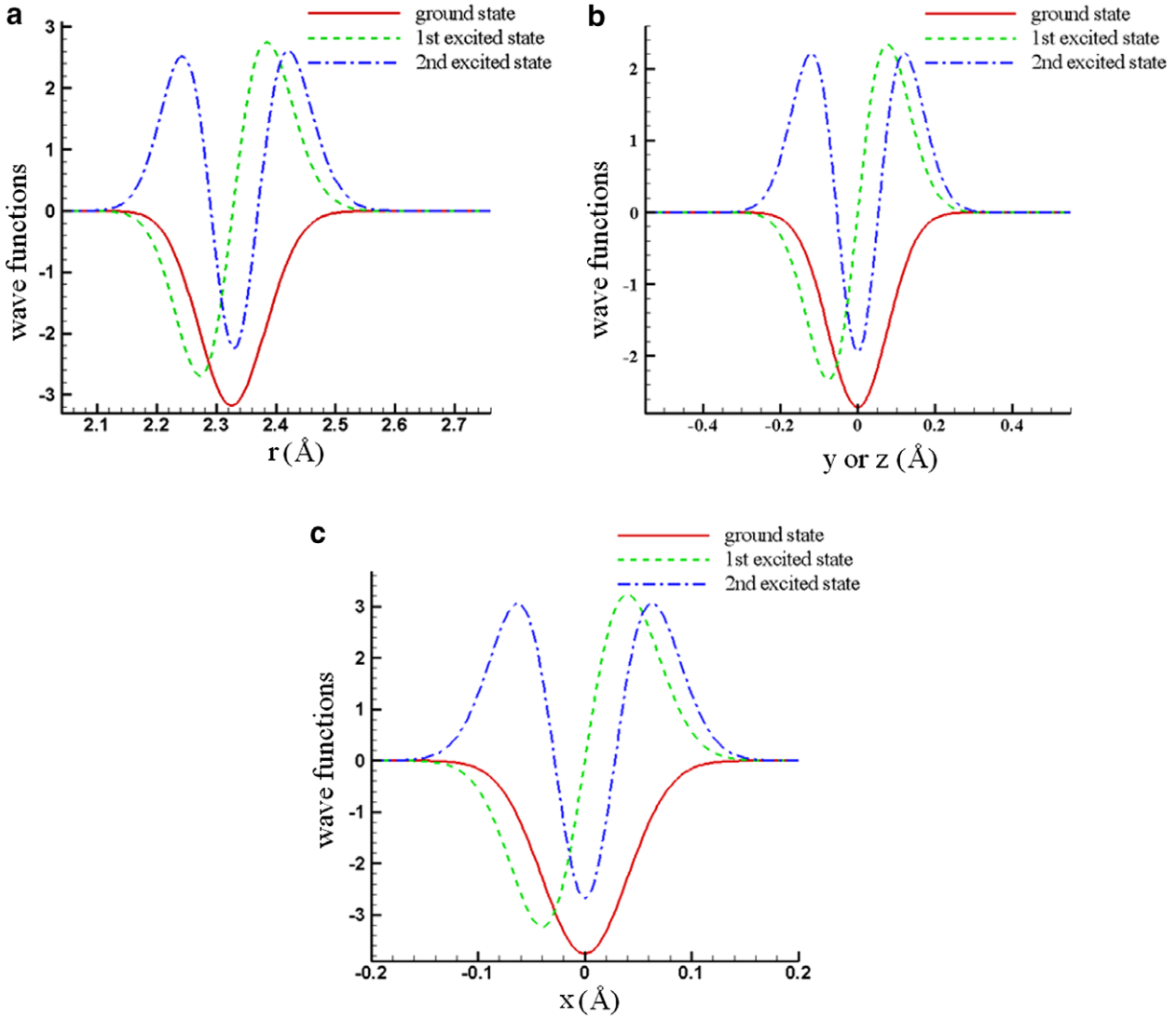

Fig. 8. The 0th order normalized vibrational wave functions of lowest three energy states, (a) symmetric stretching mode, (b) doubly degenerate bending mode, and (c) asymmetric stretching mode.

quantum number. The second and third quantum numbers n_y, n_z correspond to the two degenerate bending quantum numbers. The last one n_x corresponds to the asymmetric stretching quantum number. These eigen values and eigen functions will be used as the 0th order results of vibrational levels. The real vibrational eigen functions can be written as a linear combination of these 0th order wave functions as

$$|v\rangle = \sum_n c_{vn}|n\rangle \tag{11}$$

The coefficients c_{vn} and the real vibrational energy eigen values can be obtained by solving the following matrix equation:

$$HC_v = E_v C_v \tag{12}$$

Table 3
Energy eigen values and eigen functions of real vibration states

(v_1, v_2^l, v_3)	E(exp.)	E(cal.)	Wave functions
(0,0,0)	0	0	$0.999\|0000\rangle - 0.022\|1000\rangle - 0.015\|1200\rangle - 0.015\|1020\rangle$
$(0,1^1,0)$	667	649	$0.999\|0100\rangle - 0.015\|0300\rangle + 0.019\|1100\rangle - 0.025\|1300\rangle - 0.015\|1021\rangle$
$(0,2^0,0)$	1285	1266	$0.562\|0200\rangle + 0.562\|0020\rangle - 0.604\|1000\rangle + 0.036\|1200\rangle + 0.036\|1020\rangle$
(1,0,0)	1388	1382	$-0.427\|0200\rangle - 0.427\|0020\rangle - 0.796\|1000\rangle - 0.033\|2000\rangle - 0.024\|0000\rangle$
$(0,3^1,0)$	1932	1900	$0.644\|0300\rangle + 0.370\|0120\rangle - 0.664\|1100\rangle + 0.067\|1300\rangle + 0.037\|1012\rangle$
$(1,1^1,0)$	2077	2054	$-0.572\|0300\rangle - 0.333\|0120\rangle - 0.747\|1100\rangle - 0.045\|1300\rangle - 0.029\|1012\rangle$
(0,0,1)	2349	2372	$0.989\|0001\rangle - 0.145\|1001\rangle$
$(0,2^0,1)$	3613	3617	$0.594\|0201\rangle + 0.594\|0021\rangle - 0.528\|1001\rangle - 0.100\|2100\rangle$
(1,0,1)	3716	3745	$-0.380\|0201\rangle - 0.380\|0021\rangle - 0.812\|1001\rangle - 0.176\|2100\rangle - 0.132\|0001\rangle$

Column 1 shows the notations of the traditional CO_2 vibration levels. Columns 2 and 3 show experimental and calculated energy eigen values of CO_2 vibrations, respectively. Both of them are in unit of cm^{-1}. Column 4 shows the real vibrational wave functions expressed as linear combinations of the 0th order eigen functions $|n_r n_y n_z n_x\rangle$.

Table 4
Experimental and calculated transition dipole moments $\vec{M}_{v_1v_2}$ (Debye) of CO_2, where the sign of the transition dipole moment is arbitrary

Band	M_x(exp.)	M_x(cal.)	Band	M_y(exp.)	M_y(cal.)
Parallel bands			*Perpendicular bands*		
(0,0,1)–(0,0,0)	0.326	0.301	(0,1,0)–(0,0,0)	0.131	0.120
$(0,2^0,1)$–(0,0,0)	0.027	0.020	(1,1,0)–(0,0,0)	0.0011	0.0011
(1,0,1)–(0,0,0)	0.033	0.041	$(0,3^1,0)$–(0,0,0)	0.0005	0.0003
$(0,0,1)$–$(0,2^0,0)$	0.028	0.016	(1,0,0)–(0,1,0)	0.094	0.065
(0,0,1)–(1,0,0)	0.033	0.025	$(0,2^0,0)$–(0,1,0)	0.090	0.099
$(0,2^0,1)$–$(0,2^0,0)$	0.331	0.298	(1,1,0)–(1,0,0)	0.153	0.134
$(0,2^0,1)$–(1,0,0)	0.011	0.024	(1,1,0)–$(0,2^0,0)$	0.031	0.029
(1,0,1)–$(0,2^0,0)$	0.008	0.021	$(0,3^1,0)$–(1,0,0)	0.024	0.015
(1,0,1)–(1,0,0)	0.331	0.296	$(0,3^1,0)$–$(0,2^0,0)$	0.154	0.150

The matrix elements in the H matrix in Eq. (12) can be determined by

$$H_{mn} = H_{nm} = \langle n|\widehat{H}_0 + V|m\rangle = E_n\delta_{mn} + \langle n|V|m\rangle \tag{13}$$

where $\langle n|V|m\rangle$ is actually a four-dimensional integral which can be evaluated by repeatedly using the Simpson rule.

In the calculation, fifty 0th order wave functions corresponding to the 50 lowest 0th energy eigen values were chosen as the basis functions. So the matrix H becomes a 50×50 matrix. The matrix equation (12) was solved by matrix diagonalization schemes. Table 3 shows nine calculated real vibrational energy eigen values and eigen functions. These vibrational energy levels are related to the transitions shown in Table 4. The eigen functions in Table 3 were expressed as a linear combination of the 0th order eigen functions of which the absolute values of the coefficients are greater than 0.01.

After the real energy eigen values and eigen functions were known, the transition dipole moment between different vibrational energy levels can be calculated as

$$\vec{M}_{v_1v_2} = \left\langle v_1|\,\vec{d}(r,x,y,z)|v_2\right\rangle = \sum_{mn} c_{v_{1n}}c_{v_{2m}}\left\langle n|\,\vec{d}\,|m\right\rangle \tag{14}$$

The results are shown in Table 4. The calculated vibrational energy levels in Table 3 have generally a good agreement with the experimental data [19]. The biggest inaccuracy is less than 3%. The error is mainly caused by an approximate exchange-correlation (E_{xc}) functional used in the calculations. From the wave functions shown in Table 3, one can see (0,0,0), $(0,1^1,0)$ and (0,0,1) energy levels are dominated by their 0th order wave functions. Their real wave functions are only weakly mixed by a few other 0th order wave functions of the same species. The remaining six energy levels are originated from the three coupled vibrational levels in resonance (Fermi resonance). The 0th order wave functions of these vibrational levels are strongly mixed with 0th order wave functions of the resonant vibrational levels.

In Table 4, the transition dipole moments of nine parallel bands and nine perpendicular bands were calculated. The transition dipole moments of fundamental transition bands like (0,0,1)–(0,0,0) and (0,1,0)–(0,0,0) were dominated by only one dipolar integral in Eq. (14) because all other integrals can be neglected due to their small coefficients. For Fermi resonance energy levels, the coefficients of strongly mixed 0th order wave functions are related to two constants [19]; one is ΔE (the unperturbated separation of the energy levels in resonance, $\Delta E = E_n - E_m$) and the other is the interaction matrix elements $\langle n|V|m\rangle$ which is related to the perturbation energy V. Hence, the errors in the calculations of E_n and $\langle n|V|m\rangle$ were propagated into the calculations of coefficients c_{vn} and the transition dipole moments $\vec{M}_{v_1v_2}$ so that bigger errors may be induced. As a result, the transition dipole moments of fundamental transitions in Table 4 have generally better agreements with experimental data [20] than those of Fermi resonance levels. These results will also be improved with improved E_{xc} functionals.

4. Conclusion

Using the DFT, intra-molecular PES and DMS were determined by solving the KS equation. Appropriate supercell size and cut-off energy were selected to make a compromise between accuracy and computation speed. DFT combined with PAW potential functionals and PW basis functions greatly increased the computational speed. The DFT method predicted an excellent CO_2 geometry and fairly good vibrational energy eigen values and transition dipole moments. These results are very useful in the calculations of infrared absorption spectra of molecules. However, with the presently available potential functionals, the DFT still cannot match the accuracy that the methods like CCSD(T) and QCISD(T) can achieve [21]. It is believed if better E_{xc} functionals are available, the results would be improved by using the method developed in this paper. The high efficiency of the method developed in this paper makes it applicable to larger and more complicated molecules. However, with the number of atoms in the molecules increases, the computational cost of CCSD(T) method will be prohibitive.

Acknowledgments

This work was supported by Office of Navy Research through the Multidisciplinary University Research Initiative (MURI) program, Award No. N00014-05-1-0432.

References

[1] Z. Wang, M. Gong, Y. Zhang, E. Feng, Z. Cui, Chem. Phys. Lett. 454 (2008) 7.
[2] C. Leonard, M. Diehr, P. Rosmus, W.C. Maguire, JQSRT 109 (2008) 535.
[3] Z.G. Huang, E.C. Yang, D.Q. Xie, Chin. Chem. Lett. 19 (2008) 627.
[4] T. Stoecklin, A. Voronin, Chem. Phys. 331 (2007) 385.
[5] K.A. Peterson, G.C. McBane, J. Chem. Phys. 123 (2005) 084314.
[6] U. Lourderaj, N. Sathyamurthy, Chem. Phys. 308 (2005) 277.
[7] R. Tarroni, Mol. Phys. 102 (2004) 2167.
[8] J. Noga, R.J. Bartlett, J. Chem. Phys. 86 (1987) 7041.
[9] P.E. Blöchl, Phys. Rev. B 50 (1994) 17953.
[10] G. Kresse, J. Joubert, Phys. Rev. B 59 (1999) 1758.
[11] D.L.G. Cheung, Ph.D. Thesis, University of Durham, 2002, 33.
[12] G. Makov, M.C. Payne, Phys. Rev. B 51 (1995) 4014.
[13] W. Kohn, Phys. Rev. 140 (1965) 1133.
[14] G. Kresse, J. Furthmüller, Phys. Rev. B 54 (1996) 11169.
[15] G. Kresse, J. Furthmüller, Comput. Mater. Sci. 6 (1996) 15.
[16] E. Kaxiras, Atom. Electron. Struct. Solids (2003) 49.
[17] A.D. Buckingham, Mol. Struct. Prop. (1975) 23.
[18] T. Pang, Introduction Comput. Phys. (2006) 105.
[19] G. Herzberg, Molecular Spectra and Molecular Structure, second ed., Lancaster Press, Inc., Lancaster, PA, 1950. p. 274.
[20] I. Suzuki, J. Mol. Spectrosc. 80 (1980) 12.
[21] I.N. Levine, Quantum Chem. (2000) 591.